ISSN 2517-7516, Membranes and Membrane Technologies, 2024, Vol. 6, No. 2, pp. 71–83. © Pleiades Publishing, Ltd., 2024.

Ceramic Substrates for Filtration Membranes Based on Fine Fly Ash Microspheres

E. V. Fomenko[a], G. V. Akimochkina[a], A. G. Anshits[a], N. P. Fadeeva[a, b], I. A. Kharchenko[b], E. V. Elsuf'ev[b, c], K. A. Shabanova[d], A. A. Maksimova[c], and I. I. Ryzhkov[b, c, *]

[a] *Institute of Chemistry and Chemical Technology, Siberian Branch, Russian Academy of Sciences, Krasnoyarsk, 660036 Russia*

[b] *Institute of Computational Modelling, Siberian Branch, Russian Academy of Sciences, Krasnoyarsk, 660036 Russia*

[c] *Siberian Federal University, Krasnoyarsk, 660041 Russia*

[d] *Kirensky Institute of Physics, Siberian Branch, Russian Academy of Sciences, Krasnoyarsk, 660036 Russia*

**e-mail: rii@icm.krasn.ru*

Received October 3, 2023; revised November 10, 2023; accepted December 7, 2023

Abstract—A procedure has been proposed for producing ceramic substrates for filtration membranes based on a narrow fraction of fine fly ash microspheres using cold uniaxial pressing followed by high-temperature firing. It has been shown that increasing the sintering temperature from 1000 to 1150°C leads to a decrease in open porosity from 40 to 24%, a decrease in the average pore size from 1.60 to 0.34 μm, and an increase in the compressive strength from 9.5 to 159 MPa. The resulting substrates are characterized by water permeability values of 1210, 310, 240, 170 L m^{-2} h^{-1} bar^{-1} at sintering temperatures of 1000, 1050, 1100 and 1150°C, respectively. Experiments on filtration of aqueous suspensions of fine microspheres (d_{av} = 2.5 μm) and microsilica (d_{av} = 1.9 μm) through a substrate produced at a sintering temperature of 1150°C have shown the rejection close to 100%. The proposed methodology for using ash waste in the production of membrane materials promotes the development of technologies for the integrated processing of thermal energy waste.

Keywords: fine microspheres, fly ash, ceramic materials, filtration membranes

DOI: 10.1134/S2517751624020033

1. INTRODUCTION

Currently, the most common technologies for separating, purifying, and concentrating solutions are pressure-driven membrane processes, such as microfiltration, ultrafiltration, nanofiltration, and reverse osmosis [1]. They are characterized by high selectivity, low energy consumption, no use of chemicals, and the ease of scaling or combining with other processes [2]. Polymeric membranes with high productivity and relatively low cost are widely used in pressure-driven membrane processes [3]. Ceramic membranes, compared to polymeric ones, have a greater mechanical strength, chemical and temperature stability, the ability for regeneration, and a longer service life [4, 5]. The disadvantages of ceramic membranes include both low specific productivity due to lower packing density in modules and high production costs due to the high sintering temperature (>1300°C) of traditional precursors (alumina, silica, zirconia) [6]. In this regard, a demanding task is to reduce the cost of producing ceramic membranes through the use of more affordable materials. These include natural minerals (clay, quartz sand, perlite) and waste from the chemical and fuel-and-energy industries (in particular, fly ash containing significant amounts of aluminum oxide and silicon dioxide) [7, 8]. These materials have a complex composition and contain a number of oxides (of sodium, potassium, iron, etc.) that promote sintering at lower temperatures (<1300°C).

Ceramic membranes generally have an asymmetric structure. The coarse-porous base (substrate) provides mechanical strength and high permeability. A series of micro- and mesoporous layers are formed on the substrate surface, the thickness of which and the pore size decrease from layer to layer. The upper (selective) layer determines the separation properties of the membrane [9, 10]. One of the important tasks in the fabrication of membranes is the development of substrates from ceramic materials that provide an optimal combination of mechanical strength and liquid permeability. Increasing the sintering temperature of the starting materials usually leads to an increase in the mechanical strength of the substrate, but reduces its porosity, and, accordingly, liquid permeability [6].

Microfiltration membranes based on tubular alumina substrates with a selective layer of zirconium dioxide were obtained in [11]. The dependence of polymer additives used in applying a selective layer on

the pore size distribution and gas permeability was studied. Flat and tubular ceramic substrates and microfiltration membranes based on them were proposed in [12, 13]. Natural crystalline silica powder was used as a starting material with an aluminosilicate binder. It has been shown that the resulting membranes can be effectively used to remove ferric ions [14]. A surface modification technique has been proposed to impart antibacterial properties to membranes [15]. Ceramic membrane substrates based on Moroccan perlite powder with organic additives and water, which have high heat resistance up to 1000°C and porosity up to 40%, were obtained in [16] and [17] for flat and tubular geometry, respectively. It has been shown that these membranes can be used for treating wastewater from the leather and textile industries [18]. High-strength ceramic substrates based on perlite and foamed silicates for filtration membranes were proposed in [19]. The possibility of using bentonite clay as a starting material for producing ceramic substrates with pores in the range of 0.8–2.3 μm was demonstrated in [20]. Microfiltration membranes based on natural white clay (kaolin) have shown good performance and biocompatibility in the hemofiltration process for the separation of urea, creatinine, and phosphates from the blood [21].

As an alternative to natural minerals, materials obtained from industrial waste can be used to synthesize ceramic membranes. The combustion of coal at thermal power plants leads to a large yield of ash waste, which pollutes the environment and requires further processing [22–24]. Depending on the coal type and combustion conditions, the ash contains up to 40% finely divided particles less than 10 μm in size, consisting mainly of aluminosilicates [25]. These particles belong to anthropogenic atmospheric pollutants: suspended particulate matter PM_{10} including the particularly dangerous particles, such as $PM_{2.5}$ aerosols [26]. A significant reduction in the volume of waste ashes and environmentally hazardous particles can be achieved by involving fine microspheres of <10 μm in size in processing, since they have broad potential for the synthesis of ceramic materials with improved properties [27, 28], including membranes for filtration processes [29, 30]. The use of microspheres as a starting material can increase the permeability and reduce fouling of microfiltration membranes in such processes as the separation of oil–water emulsions or aqueous suspensions of solid particles [31, 32]. Microspheres can also be used as an additive to increase efficiency and reduce sintering temperature [33].

The purpose of this work is to develop new ceramic substrates based on narrow fractions of fine fly ash microspheres and determine their physicochemical characteristics, including strength properties and liquid permeability.

2. MATERIALS AND METHODS

As a raw material for the fabrication of ceramic filtration membranes, we used a nonmagnetic fraction of fine microspheres with a narrow size distribution of globules, isolated from alumina–silica fly ash of pulverized coal combustion. The technological separation scheme included one-stage aerodynamic classification and magnetic separation of fly ash. Aerodynamic separation was performed using a Hosokawa Alpine 50 ATP centrifugal laboratory classifier (Germany). The design of the classifier and the principle of its operation are detailed in [34, 35]. The magnetic component was extracted from the fraction in distilled water with a neodymium magnet (NdFeB, F = 24 lb). For the isolated nonmagnetic narrow fraction, bulk density, particle size distribution parameters, and chemical and phase compositions were determined. These physicochemical characteristics are the main criteria for the applicability of microspheres in the development of materials with desired properties.

Bulk density was measured using a Quantachrome Instruments Autotap automated analyzer (USA). Particle size distribution was determined using a Fritsch MicroTec 22 laser analyzer (Germany). The average globule diameter d_{av}, d_{10}, and d_{90} were calculated from three independent measurements. The absolute measurement error did not exceed ±0.3 μm.

The chemical composition of the initial narrow fraction of fine microspheres, including the concentration of silicon, aluminum, iron, calcium, magnesium, potassium, sodium, titanium, and sulfur oxides, as well as the loss on ignition, were determined by chemical analysis methods in accordance with GOST 5382–91 [36], which defines both methods for determining components and analysis accuracy standards.

The morphology of fine microspheres and ceramic substrates was studied using a Hitachi TM4000 Plus scanning electron microscope in the backscattered-electron imaging mode at accelerating voltages of 15 and 20 kV.

X-ray diffraction data were obtained on a PANalytical X'Pert ProMPD powder diffractometer (the Netherlands) with a PIXcel solid-state detector. The amount of the main crystalline phases was determined using full-profile analysis according to the Rietveld method with minimizing the difference derivative according to the procedure described in [37].

Synchronous thermal analysis (DSC–TG) was carried out in a dynamic gas mixture of 20% O_2 + 80% Ar at a total flow rate of 50 cm^3/min with simultaneous recording the mass change, heat flux, and composition of gaseous products using a Jupiter STA 449C simultaneous thermal analyzer with Netzsch Aeolos QMS 403C mass spectrometer (MS). The measurements were carried out in Pt–Rh crucibles with perforated lids in the mode of linear temperature rise at a rate of 10°C/min in the range of 40–1100°C using a

sample weight of 20.0 ± 0.2 mg. The heat flux sensitivity of the sensor was calibrated by measuring the heat capacity of a sapphire disk according to DIN 51007-2019 [38]. Primary thermoanalytical data were processed using the NETZSCH Proteus licensed software package (version 4.8.4).

In order to stabilize the chemical composition of a narrow fraction of fine microspheres, particles of unburned carbon (carbon loss in fly ash) were fired and acid treatment was carried out to remove leachable cations. Removal of unburned carbon particles was carried out at 815°C in an oxidizing atmosphere for 1 h according to a method for determining ash content [39]. Acid treatment of the narrow fraction was carried out in a mixture of concentrated nitric (HNO_3) and hydrochloric (HCl) acids, taken in a ratio of 1 : 3 by volume, for 2 h with constant stirring. The ratio of fine microspheres to a mixture of acids was 1 : 3; the etched sample was washed with water to a neutral pH value and dried at 115°C to constant weight.

The chemical composition of the samples obtained after removal of unburned carbon particles and acid etching of the narrow fraction of microspheres was determined by SEM-EDX using a Hitachi TM-4000 scanning electron microscope (SEM) equipped with a Quantax 70 microanalysis system with an Bruker XFlash 430H energy-dispersive X-ray spectrometer (EDX) according to the procedure reported in [40].

Samples of flat ceramic membranes were formed by compacting powder materials using cold static uniaxial pressing followed by high-temperature sintering [41]. Flat substrates with a diameter of 23–26 mm and a thickness of 2.5–3.5 mm were obtained at a pressure of 40 MPa in a closed rigid mold with the addition of 10% distilled water to fine microspheres. Before sintering in a muffle, the compressed samples were dried at a temperature of 115°C for 1 h to remove moisture. Firing in a muffle furnace was carried out at temperatures of 1000, 1050, 1100, and 1150°C with holding for 2 h. After sintering, the samples were polished to ensure parallelism of the upper and lower planes of the substrates. This is necessary for uniform compression of samples in holders when measuring liquid permeability, as well as during filtration experiments.

The following characteristics were determined for ceramic membrane samples: sintering ratio, apparent density, open porosity, compressive strength. These parameters conventionally characterize ceramic materials for various purposes and have been measured according to relevant GOST standards [42–44]:

(1) Sintering ratio $k_{sin} = V_2/V_1$: a dimensionless quantity defined as the ratio of the sample volume after sintering V_2 to the volume of the compressed sample V_1.

(2) Apparent density (g/cm^3): the ratio of the sample mass (g) to its total volume (cm^3) according to GOST 7025–91.

(3) Open porosity (%): the ratio of the volume of accessible pores in a sample to its total volume, the volume of accessible pores is determined by water saturation of the material according to GOST 2409–2014.

(4) Ultimate compressive strength (MPa): $\sigma_{com} = F/S$, the stress corresponding to the compressive load, at which a failure of a cylindrical test sample with a diameter of 16 mm and a height of 15 mm occurs; it is calculated as the ratio of the failure load F (N) to the transverse cross sectional area S of the sample (mm^2). The value of F was measured with an Instron 3369 universal testing machine press (USA) in accordance with GOST R 57606–2017.

The porous structure of the samples was studied using a Porolux1000 capillary flow porometer (POROMETER, Belgium). The operating principle of the porometer is based on the displacement of a wetting liquid by a gas flow with a step-by-step increase in pressure and its stabilization. Porosity analysis consists of measurements of two curves: the wet curve is measured after the sample has been soaked with a wetting liquid (Porefil, surface tension 15.9 dynes/cm), and the dry curve is measured on the same unwetted sample. The intersection point (pressure value) of the wet curve and the dry curve (taken with a coefficient of 0.5) corresponds to the average pore diameter in the sample.

The permeability of the membranes was measured using a device that pumps distilled water through the membrane under pressure. The pressure was generated by a compressor, controlled with a SMC AW20-F01C-A B pressure regulator (Japan), and monitored using a SMC ISE40A precision pressure switch (Japan). The volume of water passing through the membrane was determined using an AND GX-800 analytical balance (Japan) by automatically recording the mass after a specified period of time. The volumetric flow rate (velocity) of water J (m^3 m^{-2} h^{-1}) was calculated using the formula $J = 60V/S$, where V is the volume of water passing through the membrane per minute (m^3/min) and S is the membrane area (m^2). Permeability K was determined according to the equation

$$K = J/\Delta P, \quad (1)$$

where ΔP is the pressure upstream of the membrane (bar). For each pressure difference, measurements were made until a stable (constant) flux value was achieved.

Filtration experiments were carried out on a laboratory setup consisting of a UFC-25-400 filtration cell (Biotest, Kirishi, Russia), a compressor, a SMC AW20-F01C-A B pressure regulator, and an AND GX-4002a balance. Filtration of aqueous suspensions of SiO_2 particles (d_{av} = 1.9 μm, 200 mg/L) and microspheres (d_{av} = 2.5 μm, 200 mg/L) was carried out at a pressure of 3 bar. The concentration of particles in the

Table 1. Physicochemical characteristics of the nonmagnetic narrow fraction of fine microspheres

Bulk density, g/cm^3	Particle size distribution, μm				
	d_{av}	d_{10}	d_{50}	d_{90}	d_{99}
1.2	13.6	7.5	12.8	22.1	32.1

Chemical composition, wt %								
LOI*	SiO_2	Al_2O_3	Fe_2O_3	CaO	MgO	Na_2O	K_2O	SO_3
7.30	58.90	22.83	4.53	2.80	1.42	0.65	1.66	0.07

Phase composition, wt %				
Glass phase	Mullite	Quartz	Hematite	Calcite
91.4	4.1	3.6	0.6	0.3

* Lloss on ignition.

feed solution and permeate was determined photometrically with a Thermo Scientific Genesys 10S UV–Visible spectrophotometer. Absorbance was measured at a wavelength of 540 nm in cells with an optical path length of 50 mm. The rejection, which characterizes the filtration efficiency, was calculated using the formula:

$$R = 1 - C_p/C_f, \quad (2)$$

where C_p is the concentration of particles in the permeate and C_f is the concentration of the feed solution (mg/L).

3. RESULTS AND DISCUSSION

The nonmagnetic narrow fraction of fine microspheres used as a raw material for the synthesis of ceramic substrates for filtration membranes was characterized in detail. The bulk density value, particle size distribution parameters, and chemical and phase compositions of the fraction are given in Table 1. This fraction is characterized by a low bulk density, so that lightweight ceramic materials can expectedly be fabricated. The distribution parameters of fine particles in a narrow range of sizes indicate the homogeneity of the fraction (Fig. 1). About 1/4 of the fraction are particles with a diameter of less than 10 μm related to environmentally hazardous particular matter PM_{10}.

From the SEM image it is clear that the vast majority of particles have a spherical shape with a smooth surface, with the exception of unburned carbon particles of angular shape (Fig. 2). The small particle size of the morphologically homogeneous ash fraction makes it possible to eliminate the energy-intensive grinding stage, traditionally used in ceramic production, and thereby prevent the destruction of microspheres. In

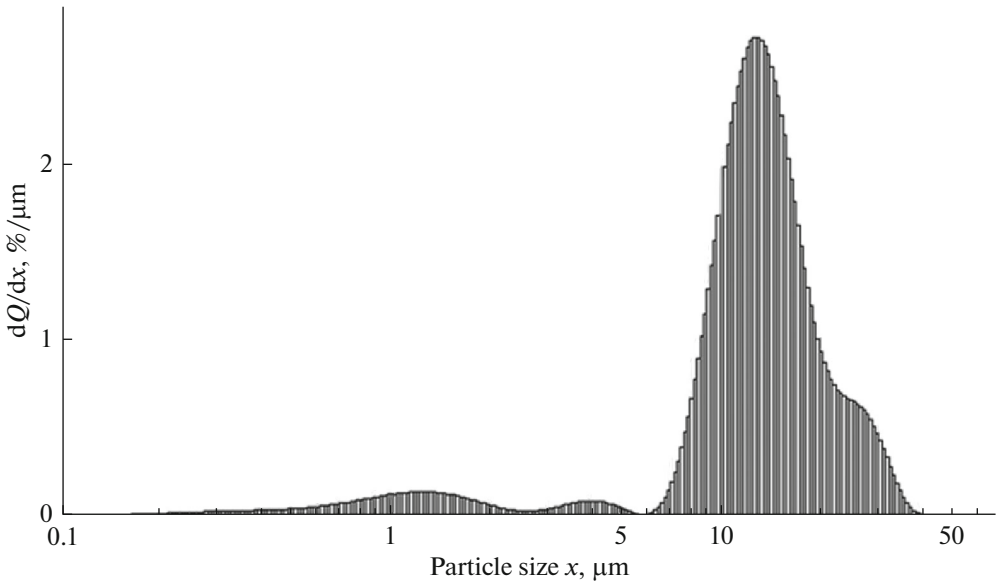

Fig. 1. Particle size distribution in differential form for a nonmagnetic narrow fraction of fine microspheres.

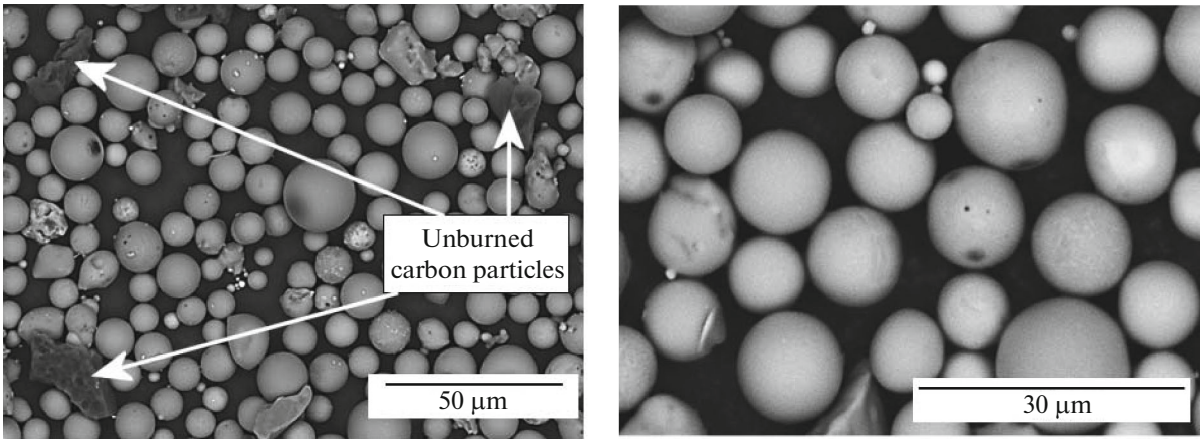

Fig. 2. SEM images of a nonmagnetic narrow fraction of fine microspheres.

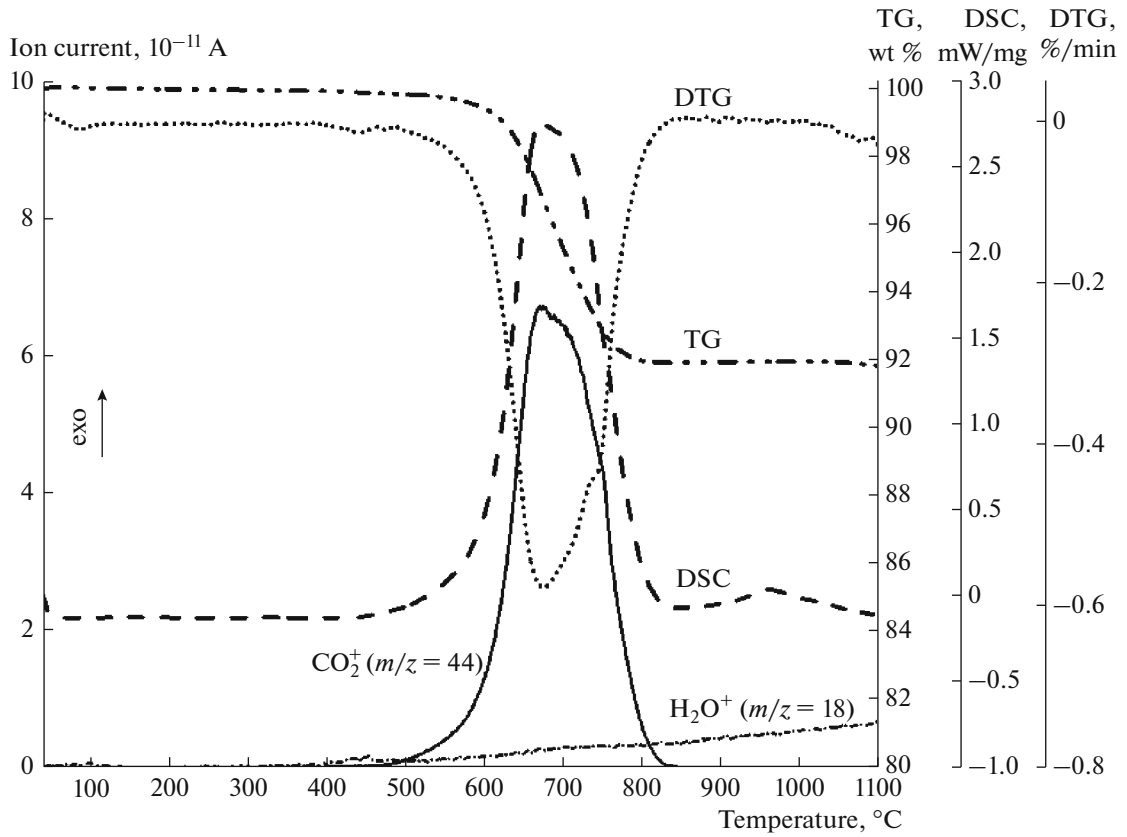

Fig. 3. DSC–TG–DTG–MS curves of thermal transformation processes for a nonmagnetic narrow fraction of fine microspheres.

turn, the preserved integrity of spherical particles ensures uniformity and appropriate packing density when compacting powder samples.

The main components of the chemical composition of the narrow fraction, as determined by chemical analysis with minimal errors, are SiO_2 and Al_2O_3, the total concentration of which reaches 82 wt %. The phase composition includes 91 wt % X-ray amorphous aluminosilicate glass phase, the crystalline phases were identified as mullite and quartz, and hematite and calcite were found at the impurity level (Table 1).

Simultaneous thermal analysis of the narrow fraction of fine microspheres showed (Fig. 3) that the following thermochemical transformations occur in the sample in the temperature range of 40–1100°C. An exothermic peak at 672°C in the DSC curve is accom-

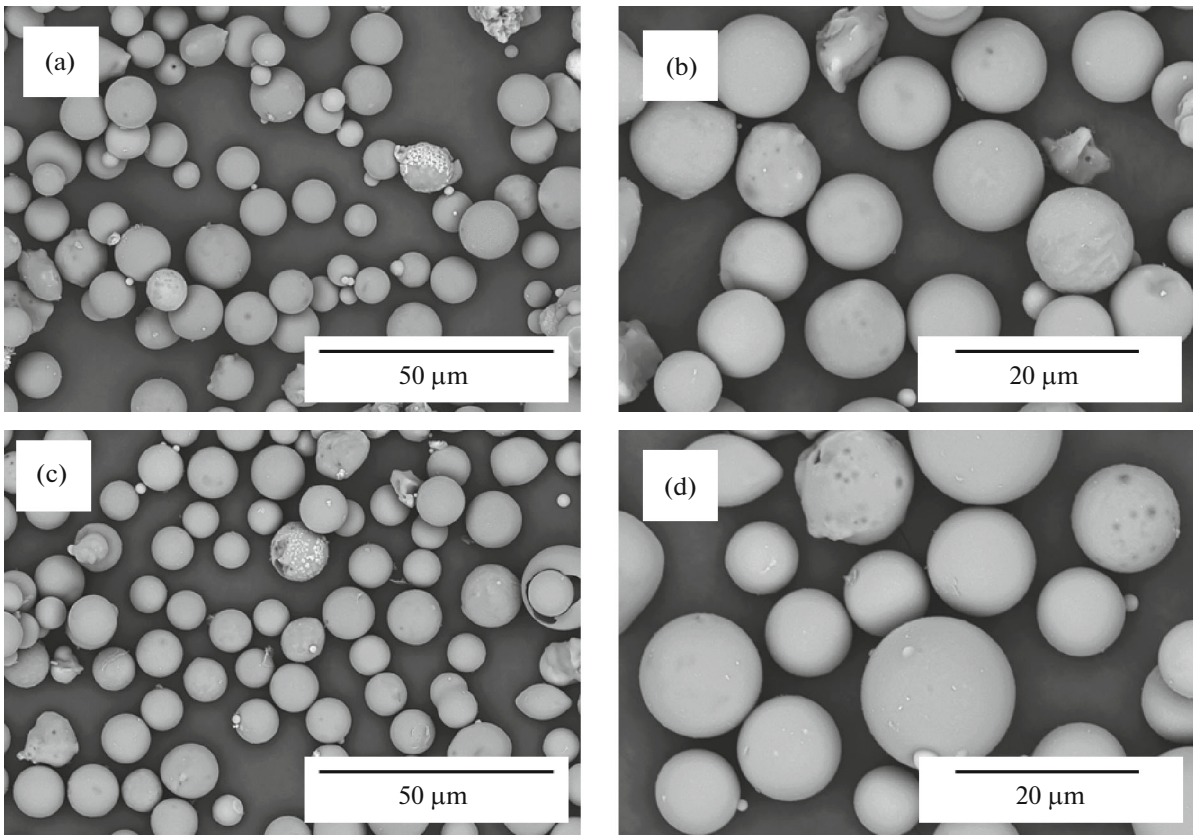

Fig. 4. SEM images of a modified nonmagnetic narrow fraction of fine microspheres after (a, b) combustion of unburned carbon and (c, d) acid treatment.

panied by a drop in mass and the release of CO_2, which is due to the combustion of unburned coal. The observed mass loss in the temperature range of 602–797°C is comparable with the LOI value determined by chemical analysis of the narrow fraction (Table 1). The second effect in the temperature range of 910–986°C with the main maximum at 962°C corresponds to the process of mullite crystallization from the aluminosilicate glass phase. At temperatures above 1030°C, the endothermic process of decomposition of impurity anhydrite $CaSO_4 \rightarrow CaO + SO_2 + 0.5O_2$ begins, which is accompanied by the release of the SO^+ fragment with $m/z = 48$.

Experiments on the fabrication of ceramic membranes based on the narrow fraction of fine microspheres without preliminary modification showed that burnout is accompanied by the release of sulfur dioxide (an increase in the intensity of the molecular ion SO_2^+ with $m/z = 64$) and unburned coal particles during the firing of molded samples leads to the formation of inner cavities and reduction of membrane strength. The presence of alkali metal and iron cations in the microspheres, which are traditional fluxes, contributes to the formation of low-melting compounds during firing, resulting in a decrease in the porosity of ceramic materials due to the formation of monolithic samples by melting. These cations can also be leached during the operation of the substrates.

To prevent these disadvantages and stabilize the chemical composition of the ash raw material, the narrow fraction of fine microspheres was subjected to modification including combustion of unburned carbon and acid treatment before the molding of ceramic membranes. The SEM images of the modified samples (Fig. 4) show that there are no angular unburned carbon particles characteristic of the parent fraction (Fig. 2). The simultaneous thermal analysis has shown (Fig. 5) that the carbon combustion peak disappears and there is a characteristic effect of crystallization of the mullite phase in the temperature range of 879–987°C with the main maximum at 958°C and the onset of crystallization of the cristobalite phase at a temperature of 1050°C. According to quantitative XRD data, after the heat treatment of the narrow fraction of fine microspheres at 1100°C, the proportions of mullite, quartz, and hematite increased to 18.7, 5.6, and 1.3 wt %, respectively; the calcite phase disappeared; and the cristobalite and anorthite phases formed in amounts of 2.3 and 5.3 wt %, respectively, with the amount of the glass phase decreasing to 66.8 wt %.

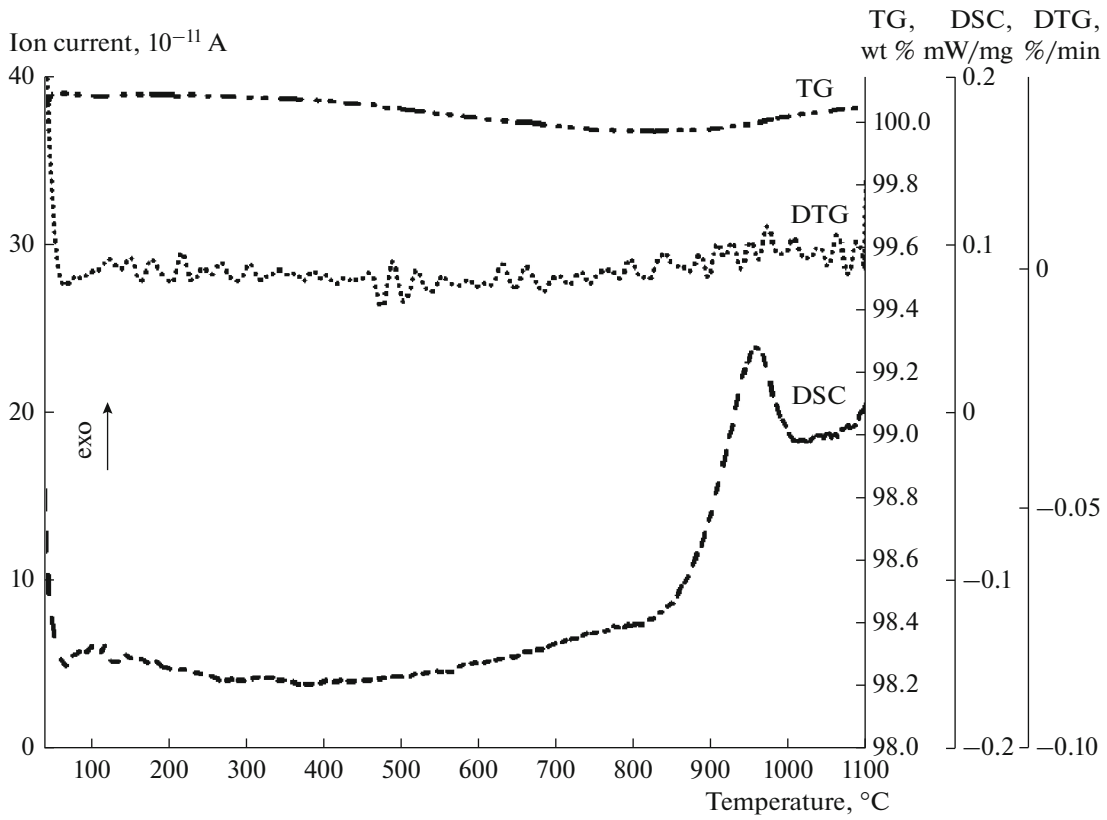

Fig. 5. DSC–TG–DTG curves of thermal transformation processes for a modified nonmagnetic narrow fraction of fine microspheres after combustion of unburned carbon and acid treatment.

Using the SEM–EDX technique, it was established that the acid treatment of the narrow fraction of fine microspheres resulted in a decrease in the concentrations of iron, magnesium, and calcium oxides by factors of ~2.5, ~2, and ~4, respectively. Thus, not only the sintering temperature of the molded samples could be elevated to 1100 and 1150°C without noticeable melting and significant loss of porosity, but also the leaching of the corresponding cations during further use of the substrates was prevented.

The main characteristics of the resulting ceramic substrates are shown in Table 2. SEM images of sections of ceramic membrane samples are shown in Fig. 6. It was found that with increasing sintering temperature, the volume of the samples noticeably decreases, as confirmed quantitatively by the sintering ratios, with the apparent density of the samples increasing. As the density increases, a decrease in porosity from 40 to 24% and a significant increase in strength from 9.5 to 159 MPa are observed. The SEM

Table 2. Main characteristics of ceramic substrates based on the modified narrow fraction of fine microspheres

Parameter	Sintering temperature, °C			
	1000	1050	1100	1150
Sintering ratio	0.84	0.76	0.68	0.64
Apparent density, g/cm^3	1.35	1.60	1.63	1.89
Open porosity, %	40	33	31	24
Ultimate compressive strength, MPa	9.5	41	98	159
Minimum pore size, μm	0.56	0.40	0.32	0.18
Average pore size, μm	1.60	1.33	0.92	0.34
Maximum pore size, μm	3.80	3.17	2.71	1.12
Liquid permeability, L m^{-2} h^{-1} bar^{-1}	1210	310	240	170

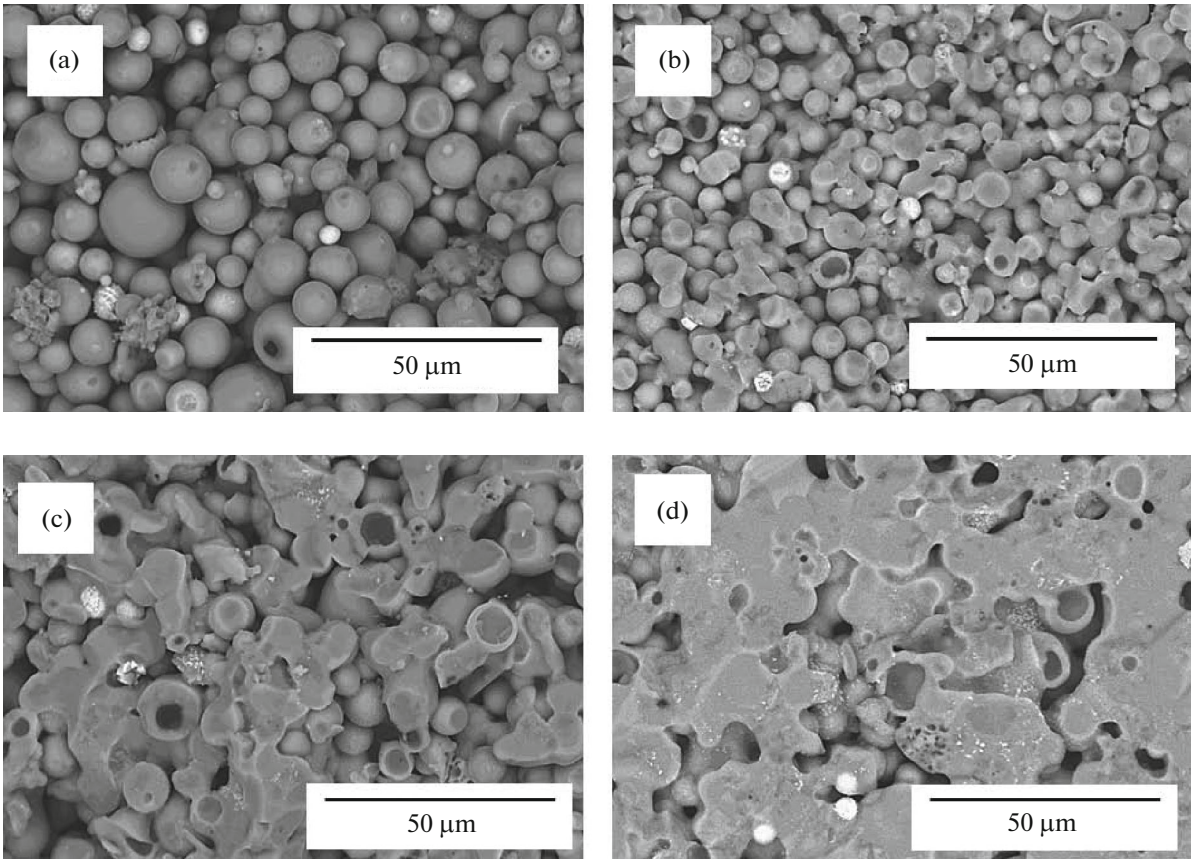

Fig. 6. SEM images of a section of ceramic substrate samples obtained on the basis of a modified narrow fraction of fine microspheres at different sintering temperatures of (a) 1000, (b) 1050, (c) 1100, and (d) 1150°C.

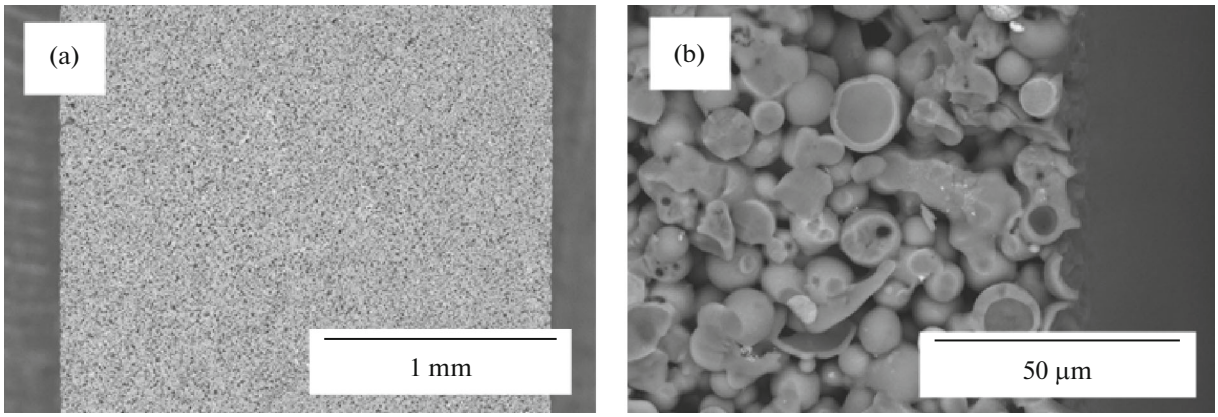

Fig. 7. SEM images of (a) a cross section of the substrate and (b) a substrate section near the surface. Sintering temperature 1100°C.

images of a cross section of the substrate indicate that it is homogeneous, without cracks and internal cavities (Fig. 7a) and the surface roughness is about 5 μm (Fig. 7b).

Figure 8 shows the pore size distributions for the samples characterized in Table 2. As can be seen, an increase in the sintering temperature leads to a shift in the maximum of the distribution function towards a smaller pore size, with the average pore size also decreasing from 1.60 to 0.34 μm (Table 2). These changes are explained by the fact that with increasing sintering temperature, fine microspheres soften to form a more developed contact surface between them.

The dependence of water flux on the transmembrane pressure in the range from 1 to 3 bar is shown in Figs. 9a and 9b, and the corresponding values of liquid

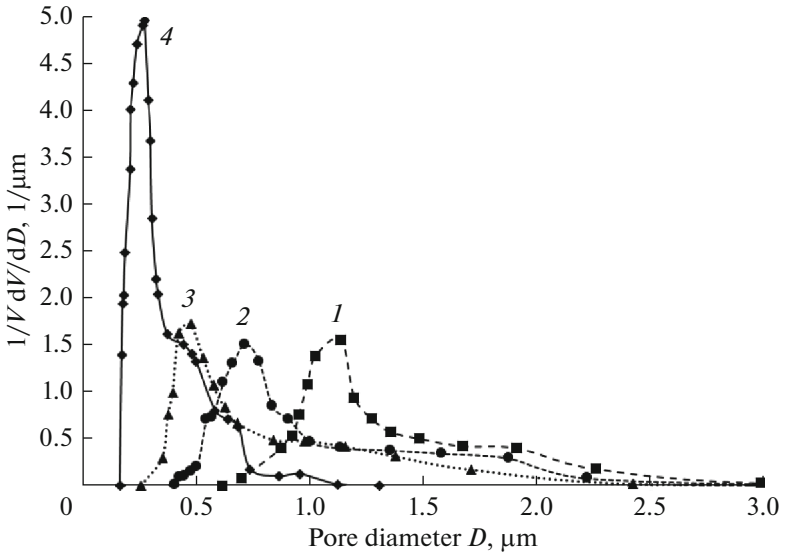

Fig. 8. Pore size distribution for substrate samples obtained at different sintering temperatures of (*1*) 1000, (*2*) 1050, (*3*) 1100, and (*4*) 1150°C.

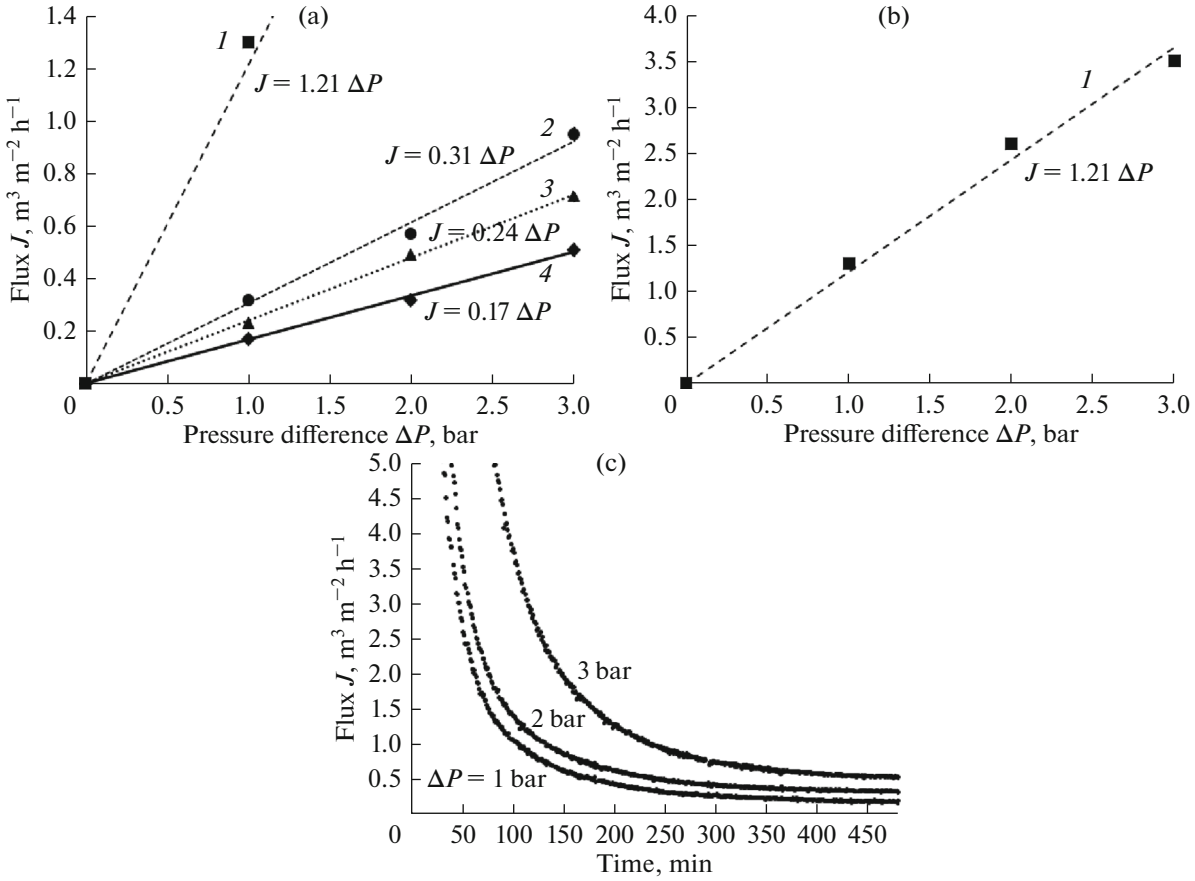

Fig. 9. (a, b) Dependence of water flux on pressure difference for substrate samples obtained at sintering temperatures of (*1*) 1000, (*2*) 1050, (*3*) 1100, and (*4*) 1150°C. (c) Time dependence of water flux for a membrane obtained at 1150°C.

Table 3. Characteristics of materials used in filtration experiments

Material	Particle size distribution, μm				
	d_{av}	d_{10}	d_{50}	d_{90}	d_{99}
Fly ash microspheres	2.5	0.8	2.0	4.8	8.3
Microsilica	1.9	0.4	1.4	4.2	8.0

permeability are given in Table 2. With an increase in the sintering temperature from 1000 to 1050°C, there is a significant drop in permeability from 1210 to 310 L m^{-2} h^{-1} bar^{-1}, with the decline in permeability being much less pronounced with the further increase in temperature. Apparently, the high permeability of the sample obtained at a sintering temperature of 1000°C is due to the presence of microcracks in it. This is indirectly evidenced by the fact that its mechanical strength is 4.3 times less than the strength of the sample obtained at 1050°C and more than an order of magnitude less than the strength of the sample corresponding to the sintering temperature of 1150°C. The time dependence of water flux for the latter sample is shown in Fig. 9c. As can be seen, the flux stabilizes over time after its sharp drop at the initial stage. A similar dependence for ceramic membranes was observed previously in a number of studies [15, 45, 46] and is associated with changes in the properties of the pore surface upon contact with water. In particular, W. Zhou et al. [45] attribute this surface change to the formation of hydrogen bonds between the polar surface groups of the glass phase and water molecules in the wall layer. As a result of this process, viscous friction increases, leading to the observed drop in the flux.

We also performed experiments on microfiltration of aqueous suspensions through synthesized ceramic substrates (membranes). Suspensions based on fractions of fine microspheres and microsilica (200 mg/L) were used, the characteristics of which are presented in Table 3. Dependences of the flux and rejection on time for a suspension of microspheres are shown in Fig. 10. The rejection is about 99.6% and almost does not change over time (average rejection values and standard deviations based on the results of three experimental runs are presented). There is a significant decrease in the flux through the membrane over time (about tenfold within 110 min), with a steady-state flux value of about 229 L m^{-2} h^{-1} at a pressure difference of 3 bar. In the case of filtering the aqueous suspension of microsilica, the rejection was initially 97.1%, but it quickly increased to 99.3% (Fig. 11). Apparently, this is due to the formation of a layer of particles on the membrane surface. In that case, too, a decrease in flux is observed over time, with its value in the steady state being 128 L m^{-2} h^{-1} at a pressure difference of 3 bar.

Note that the flux values for filtration of suspensions are significantly lower compared to the pure water flux (510 L m^{-2} h^{-1}) at the same pressure difference, see Fig. 9a.

Table 4 presents a comparison of the substrates obtained in this work (entry 1) with materials obtained in the works of other researchers in terms of the following characteristics: average pore size, open porosity, liquid permeability, compressive/flexural strength, and sintering temperature. The membranes with the closest characteristics were prepared from fly ash cenospheres (entry 2) and fly ash with the admixture of kaolin (entry 3). The addition of mullite fibers

Table 4. Physical and technical characteristics of ceramic substrates obtained in this work (1) and other studies [2–12]

No.	Substrate material	d_{av}, μm	Open porosity, %	Permeability, L m^{-2} h^{-1} bar^{-1}	Flexural/ compressive strength, MPa	Sintering temperature, °C
1	Fly ash fine microspheres (this work)	0.34–1.60	24–40	170–1210	9.5–159*	1000–1150
2	Fly ash cenospheres [47]	0.28–0.90	33–41	886–2031	8.6	1200
3	Fly ash, kaolin, dolomite [48]	0.62	46.3	468	49.4	1000
4	Fly ash, mullite [49, 50]	1–2	26.3	8298	25.1	1100
5	Fly ash, kaolin [51]	2.49	37.4	6019	16.9	900
6	Fly ash, bauxite [52]	3.4	29	5360	69.6	1300
7	Tunisian clay [53]	1.04	38	245	19	1000
8	Bentonite clay [20]	1.7	–	525	24	1000
9	Bentonite clay [54]	1.8	34	725	14.6	950
10	Clay/$CaCO_3$ [55]	3.4	52	1300	–	1250
11	Perlite [18]	1.70	52.1	1433	21.7	950
12	Perlite [16, 17]	6.64	41.8	1797	1.2	1000

* Compressive strength only.

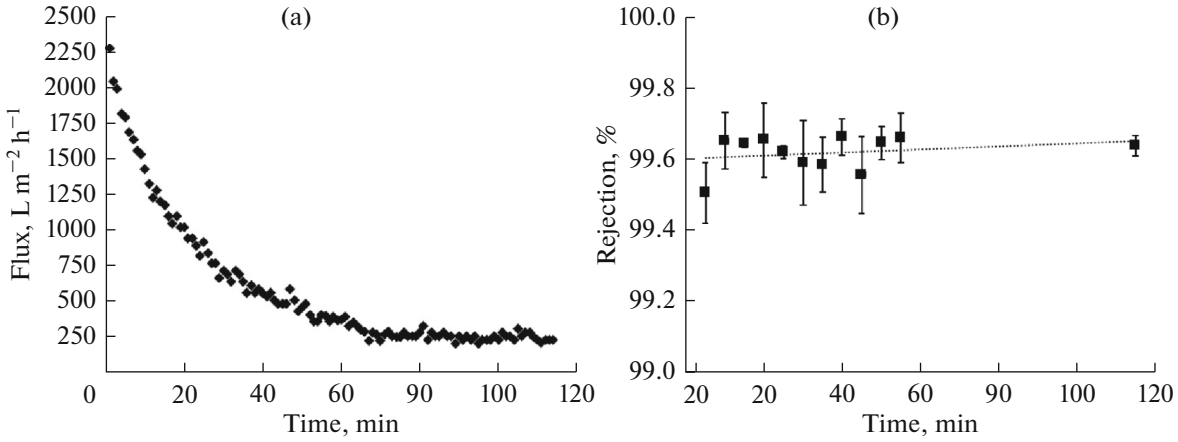

Fig. 10. Time dependence of (a) flux and (b) rejection during filtration of an aqueous suspension of fine fly ash microspheres through a substrate obtained at a sintering temperature of 1150°C.

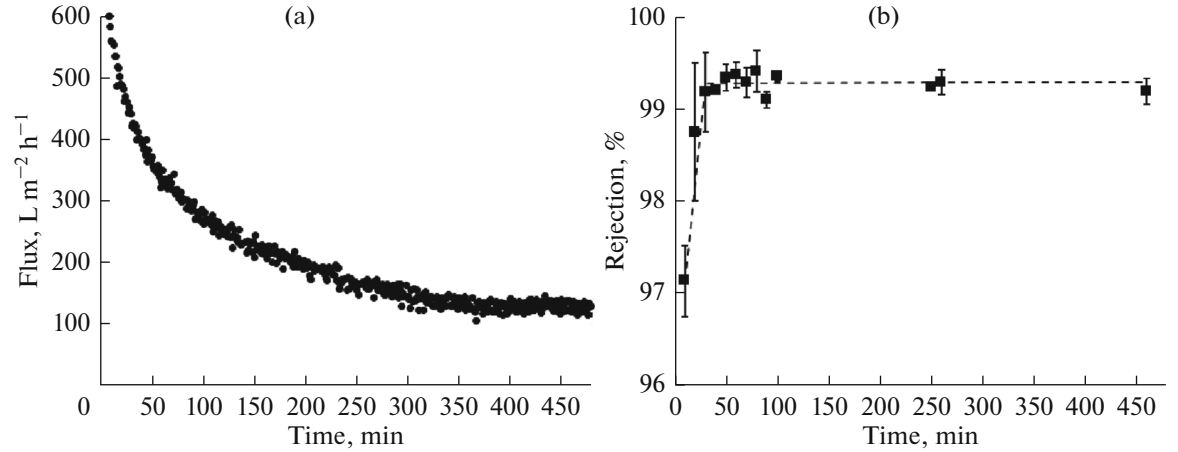

Fig. 11. Time dependence of (a) flux and (b) rejection during filtration of an aqueous suspension of microsilica through a substrate obtained at a sintering temperature of 1150°C.

or alumina particles with sizes in the range of 1–60 μm to the starting powder material made it possible to obtain membranes with increased permeability (entry 4). The higher permeability of membranes made of fly ash with the addition of kaolin or bauxite compared to those in this work is due to a larger pore size (entries 5, 6). It should be noted that within the framework of the simplest model based on the Poiseuille formula, permeability is proportional to the square of the average pore size [1]. Membrane samples made from different types of clay give comparable permeability values when corrected for pore size (entries 7–10). It is worth to note perlite-based membranes (entry 11) with high porosity (52%) and a fairly large permeability value (1433 L m^{-2} h^{-1} bar^{-1}) for an average pore size of 1.7 μm. At the same time, perlite membranes with a significantly larger pore size (6.64 μm) show a slight increase in permeability (12).

The analysis shows that the substrates obtained in this work demonstrate comparable characteristics with respect to the substrate/membrane samples described in the literature.

CONCLUSIONS

A method for producing ceramic substrates based on a narrow fraction of fine fly ash microspheres (d_{av} = 8–22 μm) has been proposed. To stabilize the chemical composition of the microspheres, unburned carbon particles were fired and acid treatment was carried out to remove leachable cations (iron, magnesium, calcium). To compact the powder material, cold static uniaxial pressing followed by high-temperature firing was used. It was found that increasing the sintering temperature from 1000 to 1150°C leads to a decrease in open porosity from 40 to 24%, a decrease in the average pore size from 1.64 to 0.34 μm, and an

increase in the compressive strength from 9.5 to 159 MPa. The resulting substrates are characterized by liquid permeability values of 1210, 310, 240, 170 L m^{-2} h^{-1} bar^{-1} at sintering temperatures of 1000, 1050, 1100 and 1150°C, respectively. Experiments on the filtration of aqueous suspensions of fine microspheres (d_{av} = 2.5 μm) and microsilica (d_{av} = 1.9 μm) through a substrate sintered at 1150°C showed rejection close to 100% and permeability in a steady state of 76.3 and 42.7 L m^{-2} h^{-1} bar^{-1}, respectively.

The resulting substrates can be used as a basis for creating micro-, ultra-, and nanofiltration membranes, including those with electrically conductive selective layers [56–58]. The use of technogenic ash waste in the production of membrane materials will help to reduce the emission of fine microparticles into the environment and create the prerequisites for the development of technologies for the integrated processing of thermal energy waste.

ACKNOWLEDGMENTS

Aerodynamic separation of fly ash was performed at the Institute of Chemistry and Chemical Technology SB RAS (project FWES-2021-0013).

FUNDING

The work was carried out with the support of the Russian Science Foundation, project no. 23-19-00269, using the equipment of the Krasnoyarsk Regional Center for Collective Use at the Krasnoyarsk Federal Research Center of the Siberian Branch of the Russian Academy of Sciences.

CONFLICT OF INTEREST

The authors of this work declare that they have no conflicts of interest.

REFERENCES

1. H. Strathmann, *Introduction to Membrane Science and Technology* (Wiley-VCH, Weinheim, Germany, 2011).
2. R. W. Baker, *Membrane Technology and Applications* (John Wiley & Sons, Chichester, England, 2004).
3. D. M. Warsinger and S. Chakraborty, et al., Progr. Polym. Sci. **81**, 209 (2018).
4. K. Li, *Ceramic Membranes for Separation and Reaction* (John Wiley & Sons, Chichester, England, 2007).
5. T. Arumugham, N. J. Kaleekkal, S. Gopal, J. K. R. Nambikkattu, A. M. Aboulella, S. R. Wickramasinghe, and F. Banat, J. Environ. Manage. **293**, 112925 (2021).
6. V. Gitis and G. Rothenberg, *Ceramic Membranes: New Opportunities and Practical Applications* (Wiley-VCH, Weinheim, Germany, 2016).
7. A. Abdullayev, M. F. Bekheet, D. A. H. Hanaor, and A. Gurlo, Membranes **9**, 105 (2019).
8. M. C. Almandoz, C. L. Pagliero, N. A. Ochoa, and J. Marchese, Ceram. Int. **41**, 5621 (2015).
9. I. P. Garmash, Yu. N. Kryuchkov, and V. N. Pavlikov, Glass Ceram. **52**, 150 (1995).
10. S. Benfer, P. Arki, and G. Tomandl, Adv. Eng. Mater. **6**, 495 (2004).
11. G. G. Kagramanov, V. V. Nazarov, E. S. Lukin, and E. M. Pershikova, Steklo Keram. **74**, 16 (2001).
12. A. I. Ivanets and V. E. Agabekov, Pet. Chem. **57**, 117 (2017).
13. A. I. Ivanets, Ves. Nats. Akad. Navuk Bel., Ser. Khim. Navuk **57**, 25 (2021).
14. A.I. Rat'ko, A. I. Ivanets, I. O. Sakhar, D. Yu. Davydov, V. V. Toropova, and A. V. Radkevich, Prot. Met. Phys. Chem. Surf **48**, 553 (2012).
15. A. I. Ivanets, T. A. Azarova, V. E. Agabekov, et al., Ceram. Int. **40**, 12343 (2014).
16. A. Majouli, S. A. Younssi, S. Tahiri, A. Albizane, H. Loukili, and M. Belhaj, Desalination **277**, 61 (2011).
17. A. Majouli, S. Tahiri, S. A. Younssi, H. Loukili, and A. Albizane, Ceram. Int. **38**, 4295 (2012).
18. S. Saja, A. Bouazizi, B. Achiou, M. Ouammou, A. Albizane, J. Bennazha, and A. Younssi, J. Environ. Chem. Eng. **6**, 451 (2018).
19. N. P. Fadeeva, M. V. Pavlov, I. A. Kharchenko, M. M. Simunin, K. A. Shabanova, V. F. Pavlov, and I. I. Ryzhkov, Membr. Membr. Technol. **4**, 170 (2022).
20. R. Chihi, I. Blidi, M. Trabelsi-Ayadi, and F. Ayari, C. R. Chimie **22**, 188 (2019).
21. R. Meghnani, M. Kumar, G. Pugazhenthi, and V. Dhakshinamoorthy, Sep. Purif. Technol. **256**, 117814 (2021).
22. Z. T. Yao, X. S. Ji, P. K. Sarker, J. H. Tang, L. Q. Ge, M. S. Xia, and Y. Q. Xi, Earth-Sci. Rev. **141**, 105 (2015).
23. M. Ahmaruzzaman, Progr. Energy Combust. Sci. **36**, 327 (2010).
24. R. S. Blissett and N. A. Rowson, Fuel **97**, 1 (2012).
25. N. Moreno, X. Querol, J. M. Andres, K. Stanton, M. Towler, H. Nugteren, M. Janssen-Jurkovicova, and R. Jones, Fuel **84**, 1351 (2005).
26. P. Thangavel, D. Park, and Y. C. Lee, Int. J. Environ. Res. Public Health **19**, 7511 (2022).
27. S. Wang, C. Zhang, and J. Chen, J. Mater. Sci. Technol. **30**, 1208 (2014).
28. T. F. Choo, SallehM. A. Mohd, K. Y. Kok, K. A. Matori, and S. Abdul Rashid, Materials **13**, 5218 (2020).
29. Z. Wei, J. Hou, and Z. Zhu, J. Alloys Compd. **683**, 474 (2016).
30. J. Huang, H. Chen, J. Yang, T. Zhou, and H. Zhang, Ceram. Int. **49**, 15655 (2023).
31. J. Fang, G. Qin, W. Wei, and X. Zhao, Sep. Purif. Technol. **80**, 585 (2011).
32. J. Fang, G. Qin, W. Wei, X. Zhao, and L. Jiang, Desalination **311**, 113 (2013).
33. D. Zou, X. Chen, E. Drioli, M. Qiu, and Y. Fan, Ind. Eng. Chem. Res. **58**, 8712 (2019).
34. O. A. Kushnerova, G. V. Akimochkina, E. V. Fomenko, E. V. Rabchevskii, and A. G. Anshits, Solid Fuel Chem. **52**, 188 (2018).

35. E. V. Fomenko, N. N. Anshits, O. A. Kushnerova, G. V. Akimochkina, S. V. Kukhtetskiy, and A. G. Anshits, Energy Fuels **33**, 3584 (2019).
36. GOST (State Standard) 5382–2019, *Cements and Materials for Cement Production* (Moscow, 2019).
37. E. Fomenko, N. Anshits, L. Solovyov, O. A. Mikhaylova, and A. G. Anshits, Energy Fuels **27**, 5440 (2013).
38. DIN 51007-2019. *Thermal analysis, Differential Thermal Analysis (DTA) and Differential Scanning Calorimetry (DSC), General Principles*.
39. GOST (State Standard) R 55661–2013, *Solid Mineral Fuel. Determination of Ash Content* (Moscow, 2014).
40. E. V. Fomenko, N. N. Anshits, L. A. Solovyov, Y. V. Knyazev, S. V. Semenov, O. A. Bayukov, and A. G. Anshits, ACS Omega **6**, 20076 (2021).
41. S. J. Glass and K. G. Ewsuk, MRS Bull. **22**, 24 (1997).
42. GOST (State Standard) 7025–91, *Ceramic and Silicate Bricks and Stones* (Moscow, 2006).
43. GOST (State Standard) 2409–2014, *Refractories. Method for Determining Apparent Density, Open and Total Porosity, Water Absorption* (Moscow, 2014).
44. GOST (State Standard) R 57606–2017, *Ceramic composites. Compression test method at normal temperature*.
45. W. Zhou, L. Zhang, P. Wu, Y. Cai, X. Zhao, and C. Yao, Materials **12**, 2161 (2019).
46. M. I. M. Esham, A. L. Ahmad, and M. H. D. Othman, Membranes **11**, 739 (2021).
47. W. Zhou, L. Zhang, P. Wu, Y. Liu, Y. Cai, and X. Zhaoa, J. Hazard. Mater. **400**, 123183 (2020).
48. N. Malik, V. K. Bulasara, and S. Basu, Ceram. Int. **46**, 6889 (2020).
49. D. Zou, M. Qiu, X. Chen, E. Drioli, and Y. Fan, Sep. Purif. Technol. **210**, 511 (2019).
50. D. Zou, W. Fan, J. Xu, E. Drioli, X. Chen, M. Qiu, and Y. Fan, J. Membr. Sci. **621**, 118954 (2021).
51. A. Agarwal, A. Samanta, B. K. Nandi, and A. Mandal, J. Pet. Sci. Eng. **194**, 107475 (2020).
52. W. Fan, D. Zou, J. Xu, X. Chen, M. Qiu, and Y. Fan, Membranes **11**, 711 (2021).
53. S. Fakhfakh, S. Baklouti, S. Baklouti, and J. Bouaziz, Adv. Appl. Ceram. **109**, 31 (2010).
54. A. Bouazizi, M. Breida, A. Karim, B. Achiou, M. Ouammou, J. I. Calvao, A. Aaddane, K. Khiat, and S. Alami Younssi, Ceram. Int. **43**, 1479 (2017).
55. F. Bouzerara, A. Harabi, B. Ghouli, N. Medjemem, B. Boudaira, and S. Condom, Proc. Eng. **33**, 278 (2012).
56. D. V. Lebedev, A. V. Shiverskiy, M. M. Simunin, V. S. Solodovnichenko, V. A. Parfenov, V. V. Bykanova, S. V. Khartov, and I. I. Ryzhkov, Pet. Chem. **57**, 306 (2017).
57. D. V. Lebedev, V. S. Solodovnichenko, M. M. Simunin, and I. I. Ryzhkov, Pet. Chem. **58**, 474 (2018).
58. I. I. Ryzhkov, M. A. Shchurkina, E. V. Mikhlina, M. M. Simunin, and I. V. Nemtsev, Electrochim. Acta **375**, 137970 (2021).

Translated by S. Zatonsky